BJES Basrah Journal for Engineering Sciences

Basrah Journal for Engineering Sciences, Vol. 24, No. 2, (2024), 12-23

Original Article

Journal homepage: www.bjes.edu.iq
ISSN (Online): 23118385, ISSN (Print): 18146120

Simulation of the Effect of Soil Temperature on Earth - Air Heat Exchanger Behavior

Hussam Hakeem Qasim [1, *], Ahmed K. Alshara [2], Falah A. Abood [3]

[1,3] *Department of Mechanical Engineering, College of Engineering, University of Basrah, Basrah, Iraq*
[2] *Department of Mechanical Engineering, College of Engineering, University of Misan, Misan, Iraq*
E-mail addresses: pgs.hussam.hakeem@uobasrah.edu.iq , dr.ahmed_alshara@uomisan.edu.iq , falah.abood@uobasrah.edu.iq
Received: 6 May 2024; Accepted: 29 May 2024; Published: 17 August 2024

Abstract

Modern life makes energy, and the source of it is very important. This renewable energy comes from the Earth-Air Heat Exchanger (EAHE) in the soil employed as an air conditioning device for buildings in the climate conditions in Basrah city, south of Iraq. In the present study, the EAHE buried in the soil is simulated numerically using the finite volume method with a soft package. ANSYS: Fluent 2021/R2. A parametric analysis was carried out to determine the effect of three depths (Z = 1, 2, and 3 m), taking into account the physical properties of the soil in the area under study, which is in the city of Basrah in southern Iraq, at longitude 47.749° and latitude 30.568°, as well as the data and time of 1/6/2023 at 12 p.m., the diameter of the pipe (D = 7.62, 10.16, and 15.24 cm), and different velocities (v = 0.5, 1, and 1.5 m/s). The results are presented as a temperature contour and a velocity contour for the performance of EAHE. The important results showed that when the depth of the buried pipe decreases, the temperature of the air outlet and heat exchanger increases; when the diameter decreases, the air outlet temperature from the EAHE and the soil temperature decrease; when the length of the pipe is about 30 m, after this length, the decrease in temperature is very small; and the maximum temperature difference of about 10 °C between the ambient temperature and the outlet temperature of the EAHE was obtained at a depth of 3 m and a velocity of 1 m/s at a diameter of 7.62 cm.

Keywords: Earth-Air heat exchanger, Soil temperature simulation, Buried pipe, Temperature distribution for pipe.

https://doi.org/10.33971/bjes.24.2.3

1. Introduction

The earth-air heat exchanger represents a modern solution for controlling temperatures by harnessing the earth's natural temperature. As air traverses through these conduits, it undergoes cooling or heating, influenced by the subsurface temperature. This preliminary conditioning optimizes the temperature of air entering buildings, thereby reducing the energy demand for thermal regulation, be it heating or cooling via solar collectors. To enhance heat transfer efficiency, subterranean heat exchangers are integrated into the system. These consist of a network of pipes embedded within thermally conductive mediums like sand, clay, or concrete, facilitating smoother and more efficient heat transfer, consequently maintaining a consistent temperature within the solar collector and enhancing cooling performance.

Prior research indicates that the cooling efficiency of the buried pipes is contingent upon four key parameters: [1]

1. Length of the pipe.
2. Diameter or radius of the pipe.
3. Depth of pipe insertion into the ground.
4. Airflow rate within the pipe.

Studies reveal that the outlet temperature of the buried pipes decreases as the length increases, the diameter decreases, the airflow rate diminishes, and the depths increase, particularly up to 4 meters [2]. Furthermore, the majority of research utilizes various simulation tools alongside experimental data, underscoring the importance of simulation methodologies in predicting and comprehending the intricate behavior of earth-air heat exchangers.

Belatrache et al. [3] a numerical investigation was conducted to model earth-air heat exchangers (EAHE) in Adrar, Algeria, aiming to determine the optimal burial depth for pipes. Factors considered included pipe length, radius, and airflow velocity. Results indicated that a burial depth of 5 m was ideal, based on a standardized annual soil temperature profile generated using MATLAB. showed a temperature decline from a peak of 45 °C in July to around 25 °C. The temperature difference between ambient air and the heat exchanger outlet in July was calculated at 20.7 °C. Additionally, the analysis revealed significant temperature reduction within the heat exchanger, reaching equilibrium with the soil temperature along a pipe length of about 25 m. Poshtiri and Zamiri [4] achieved a numerical investigation of the ability of the solar chimney and EAHE to provide for the thermal needs of individuals, to achieve the best system performance. The results showed the best performance of the EAHE design with a diameter of 0.5 m, a length of less than 35 m, and an air gap size of 0.2 m for the solar chimney. Hammadi and Mohammed [5] study on solar chimneys with EAHE in Basrah aimed to reduce energy consumption and indoor heat in hot seasons. The 6.3 FLUENT program code was used to predict outside air temperature and cooling. Results showed that outlet air temperature decreases with pipe length and remains constant over 70 meters. Reducing pipe diameter improves heat transfer and reduces soil temperature. The soil

temperature stabilizes after 4 meters, with a maximum temperature drop of 11°C at 1 meter.

Li et al. [6] examined a passive air conditioning system that combines a solar collector with EAHEs. Findings demonstrated that the integrated system effectively sustains optimal indoor thermal conditions within the acceptable range specified by the ASHRAE standard for thermal comfort. Moreover, as the outdoor air temperature and solar radiation escalate, the solar chimney's natural draft intensifies, resulting in increased airflow into the building. Haghighi and Maerefat [7] conducted a numerical investigation on the design of a solar chimney coupled with EAHE. They determined that optimal performance is achieved with EAHEs featuring a diameter of 0.5 m and a length of 25 m. This configuration ensures thermal comfort standards are met even under low solar radiation conditions (as weak as 250 W/m^2) and when outside air temperatures drop to 0 ℃. Furthermore, they concluded that a heat exchanger longer than 35 m may not yield significant benefits. Serageldin et al. [8] introduced a relationship linking ventilation rate, solar chimney design factors, EAHE geometrical characteristics, and climatic conditions in hot arid regions. This correlation was applied in a case study involving the passive cooling, heating, and ventilation of a two-story residential structure in Egypt through TRNSYS simulation. The results of the baseline scenario indicated that zone temperatures consistently exceeded ambient temperatures throughout the year. However, with the implementation of the proposed system, zone temperatures were reduced by approximately 5 °C to 9 °C compared to ambient temperatures during the summer season. Ahmed et al. [9] studied the EAHEs physical and hybrid modelling techniques to reduce energy consumption. The results showed that the hybrid modelling is more effective than the physical modelling, but the hybrid models are more complex when developing the model, taking into consideration the operating conditions of EAHE and other parameters. Physical models need less training data for the purpose of developing the model, while hybrid models need medium data. Mostafaeipour et al. [10] conducted a theoretical and economic assessment of EAHE energy performance through natural ventilation in hot, arid regions. Investigated three pipe lengths (25, 50, and 75 m) and varying burial depths (1, 2, and 3 m). Findings show that the heat exchanger reduced summer inlet air temperatures by 0.5 °C to 9.9 °C while raising them by 0.9 °C to 11.2 °C in winter, and that increasing both pipe length and burial depth enhanced the heat exchanger's efficiency. However, pipe lengths below 25 m had minimal impact on temperature, and employing pipes longer than 75 m did not significantly enhance cooling. Essa and Hammadi [11] investigated the impact of environmental factors on the flow characteristics of aboveground and underground pipelines using PCM and a helical heat exchanger. Finding that the effect of solar radiation is more significant than ambient temperature or wind speed, and the diameter of the pipeline significantly affects the fluid temperature. Studied numerically and experimentally of a solar energy tower with an underground heat exchanger in Tikrit city, Iraq, by Abed et al. [12]. The results showed that at a depth of 3 m and an outer diameter of 152 mm, this is the maximum efficiency of the heat exchanger, and the temperature is constant and is approximately 21℃. When the air velocity is increased, the air exit temperature from the heat exchanger increases and ranges from 22.2 to 28 ℃. The pipe outlet temperature for air increases with the increase in the pipe diameter and decreases with the increase in the length and depth of the pipe, and the average air temperature decrease is 12-18 °C. Serageldin et al. [13] conducted experimental research and parametric analysis on a passive solar chimney heating and ventilation system incorporating EAHE. Discovered that the diameter of the EAHE pipe exhibited the highest sensitivity. Additionally, observed that increasing the depth led to fewer fluctuations in soil temperature, with stability or minimal variations occurring when the depth exceeded 2 m during certain times of the year. Furthermore, finding that the diameter of the EAHE is a crucial factor for pressure drop and flow rate increase.

This paper presents a simulation of an earth-air heat exchanger in Basrah, Iraq, utilizing the ANSYS-Fluent 2021/R2 program. The aim of the current study is to obtain the lowest temperature leaving the heat exchanger using the soil temperature by studying several parameters such as the diameter of the pipe, burial depth for the pipe, and for different air velocities, the continuity equation, momentum equations, and energy equations of air are solved, as well as the temperature distribution of the air in the pipe and the soil and the velocity distribution inside the heat exchanger.

2. Mathematical formulation

2.1. Geometrical models

Three models of the earth-air heat exchanger were simulated, buried at different depths and at different velocities in the conditions of the city of Basrah, Iraq, as shown in Fig. 1, which shows the earth-air heat exchanger with its dimensions. A three-dimensional model was used to describe the earth-air heat exchanger of forced ventilation. The pipe from PVC (Polyvinyl Chloride) pipe buried in the ground has different geometric parameters used in the thermal analysis: different diameters (D = 7.62, 10.16, and 15.24 cm), different depths (Z = 1, 2, and 3 m) for different velocities, and a thickness of usually 4 mm. All the models have the same dimensions. The physical and thermal specifications of air, soil, and pipe used in the theoretical simulation analysis of the models are represented in Table 1.

The principle of operation of the heat exchanger is that air is drawn from the outside and enters the room in the case of connecting a solar chimney, which is called natural ventilation, or the air is pumped by a suitable fan and is called forced ventilation, where the air is cooled by transferring heat to the soil. The air is cooled by transferring heat from the air inside the pipe to the soil, where the soil temperature is lower than the temperature entering the air in the summer or in the hot months. The above configuration can be simplified by considering that the soil surrounding the heat exchanger has constant and uniform thermal properties and that the physical dimensions of the pipe are considered constant. The model is based on energy balance equations when the soil temperature is constant. The equation takes into account the following parameters along the heat exchanger that describe the change in air temperature:

1. Outside temperature (ambient air).
2. Soil temperature at a certain depth, taking into account the thermophysical properties of the soil.
3. Geometry, pipe type and air velocity.

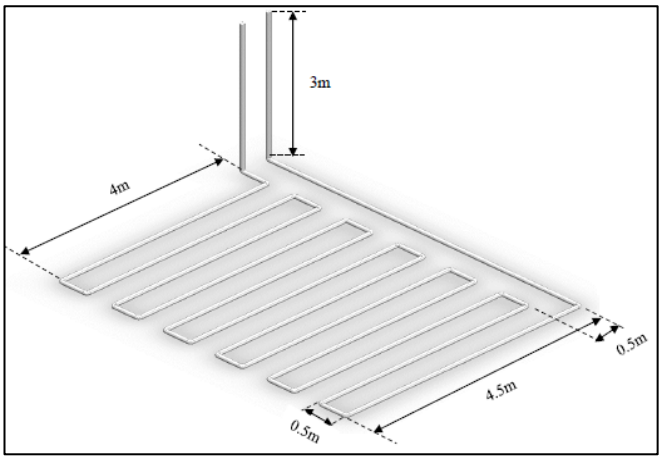

Fig. 1 Schematic of Earth-Air Heat Exchanger.

Table 1. Physical and thermal properties [8].

Materials	Density (ρ) (kg/m^3)	Thermal conductivity (k) (W/m.K)	Specific heat capacity (C_P) (J/kg.K)
PVC	1380	0.16	900
Air	1.225	0.0242	1005
Soil	2050	0.52	1840

2.2. The governing equations

The airflow within the earth-air heat exchanger is driven by forced convection, induced by an external factor like a small fan. The simulation employs governing equations, including mass conservation for the Reynolds Averaged Navier-Stokes (RANS) equations and momentum equation, as well as equations for energy, turbulence, and radiation transfer. These equations (continuity, momentum, and energy) were solved under various assumptions to solve the current flow and heat transfer cases within the system. The assumptions for the EAHE are outlined as follows:

- Steady-state conditions.
- Turbulent flow.
- Three-dimensional model.
- Density in buoyancy force is modeled by Boussinesq approximation is utilized.
- The flow is incompressible.
- The soil is considered as a homogeneous medium and isotropic.
- All the air properties are constant and they are evaluated at ambient temperature T_a = 313 K, T_s = 304.578 K, and T_{soil} = 297.487 K.
- Viscous dissipation and compression work are assumed negligibly small.
- The EAHE located at 30.568738° latitude and longitude 47.749277°.

The governing equations are a set of Kronecker symbol δ_{ij}, for continuity, momentum, and energy equations as shown below [14]:

- **Continuity equation**

$$\frac{\partial \rho}{\partial t} + \frac{\partial u_i}{\partial x_i} = 0 \tag{1}$$

- **Momentum equation**

$$\rho \frac{Du_i}{Dt} = -\frac{\partial P}{\partial x_i} + \frac{\partial}{\partial x_j}\left[\mu\left(\frac{\partial u_i}{\partial x_j} + \frac{\partial u_j}{\partial x_i}\right) - \rho\overline{u_i u_j}\right] + \rho g_i \beta(\mathrm{T} - \mathrm{T_a}) \tag{2}$$

- **Energy equation**

$$\rho C_P \frac{DT}{Dt} = \frac{\partial}{\partial \mathrm{x_j}}\left[k\frac{\partial T}{\partial x_j} - \rho C_P \overline{u_j T}\right] \tag{3}$$

$$\frac{DT}{Dt} = \frac{\partial}{\partial x_j}\left[\frac{k}{\rho C_P}\frac{\partial T}{\partial x_j} - \overline{u_j T}\right] \tag{4}$$

$$\frac{DT}{Dt} = \frac{\partial}{\partial x_j}\left[\alpha\frac{\partial T}{\partial x_j} - \overline{u_j T}\right] \tag{5}$$

$$\alpha = \frac{k}{\rho C_P} \tag{6}$$

Where,

$$\frac{D}{Dt} = \frac{\partial}{\partial t} + u\frac{\partial}{\partial x} + v\frac{\partial}{\partial y} + w\frac{\partial}{\partial z} \tag{7}$$

$$\frac{DT}{Dt} = \frac{\partial T}{\partial t} + u\frac{\partial T}{\partial x} + v\frac{\partial T}{\partial y} + w\frac{\partial T}{\partial z} \tag{8}$$

$x_j = x, y, z$ and $u_j = u, v, w$

know the finial energy equation becomes:

$$\frac{\partial T}{\partial t} + u\frac{\partial T}{\partial x} + v\frac{\partial T}{\partial y} + w\frac{\partial T}{\partial z} = \frac{\partial}{\partial x}\left(\alpha\frac{\partial T}{\partial x}\right) + \frac{\partial}{\partial y}\left(\alpha\frac{\partial T}{\partial y}\right) + \frac{\partial}{\partial z}\left(\alpha\frac{\partial T}{\partial z}\right) \tag{9}$$

The equation (7) is called the material derivative [15]. α: thermal diffusivity is the buoyancy source or sink term. u_i is the velocity component in the directions X_i, X_j, T, and P, temperature and pressure, respectively. μ is viscosity, which is turbulent Reynold's stress. The turbulent heat transfer is evaluated by an opposite turbulence model. By adopting the eddy or turbulent viscosity models, they are calculated as [17]:

- **Turbulent Reynolds stresses:**

$$-\rho\overline{u_i u_j} = \mu_t\left(\frac{\partial u_i}{\partial x_j} + \frac{\partial u_j}{\partial x_i}\right) - \frac{2}{3}\rho k\delta_{ij} \tag{10}$$

- **Turbulent heat transfer:**

$$-\rho\overline{u_j T} = \frac{\mu_t}{Pr_i}\frac{\partial T}{\partial x_j} \tag{11}$$

Where: μ_t is the turbulent dynamic viscosity, Pr the Prandtl number. δ_{ij} Kronecker delta, $\delta_{ij} = 1$ if $i = j$ and $\delta_{ij} = 0$ if $i \neq j$.

The unaltered temperature of the earth plays a crucial role in the design of a heat exchanger system, under the assumption of soil homogeneity and consistent thermal diffusion. Consequently, the temperature, as well as the depth, can be estimated at any given time using the following equation [17]:

$$T_{z,t} = T_m - A_s exp\left[-Z\left(\frac{\pi(\text{rad.})}{365\alpha_s}\right)^{\frac{1}{2}}\right]\cos\left\{\frac{2\pi(\text{deg.})}{365}\left[t - t_\circ - \frac{Z}{2}\left(\frac{365}{\pi\alpha_s}\right)^{\frac{1}{2}}\right]\right\} \quad (12)$$

And the energy equation for the soil:

$$\frac{\partial^2 T_{soil}}{\partial x^2} + \frac{\partial^2 T_{soil}}{\partial y^2} + \frac{\partial^2 T_{soil}}{\partial z^2} = \frac{1}{\alpha_s}\frac{\partial T_{soil}}{\partial t} \quad (13)$$

where: $T_{z,t}$ is the earth's temperature at time t (day), T_m is the average soil surface temperature (℃), A_s is the extent of soil surface variation was (12 ℃), Z is the depth (m), α_s is the soil thermal diffusivity was (0.0038 m^2/h), t is the time elapsed from the beginning of the calendar year (day), and t_o phase constant of the soil surface was (23 day) [5].

Calculating the undisturbed ground temperature presents a challenge due to the largely unknown soil parameters, typically defined by average soil properties. As a result, the undisturbed ground temperature remains hypothetical, equivalent to the annual average temperature of the soil surface in a specific area. Assuming that the ambient air temperature is equal to the soil surface temperature, the undisturbed ground temperature in Basrah (southern Iraq) is estimated at 24.4 °C, mirroring the region's average annual temperature [5], [18].

3. Turbulence model (standard *k-ε*)

Various turbulence models employ the notion of turbulent viscosity or turbulent diffusion to represent turbulent heat fluxes and Reynolds stresses. This yields a time-average equation for turbulent flow that resembles the laminar flow equations, with distinctions arising when laminar coefficients such as diffusion and viscosity are substituted by effective coefficients encompassing both turbulent and laminar effects [19].

The standard *k-ε* model stands as the predominant turbulence model, comprising two equations governing kinetic energy (k) and its dissipation rate (ε). Characterized by these parameters, the turbulence model is employed in the current study. It establishes a relationship between turbulent quantities and local values of density (ρ), kinetic energy (k), and dissipation rate (ε) through the following expression [19]:

$$\frac{\partial}{\partial x}(\rho uk) + \frac{\partial}{\partial y}(\rho vk) + \frac{\partial}{\partial z}(\rho wk) = \frac{\partial}{\partial x}\left(\frac{\mu_t}{\sigma_k}\frac{\partial k}{\partial x}\right) + \frac{\partial}{\partial y}\left(\frac{\mu_t}{\sigma_k}\frac{\partial k}{\partial y}\right) + \frac{\partial}{\partial z}\left(\frac{\mu_t}{\sigma_k}\frac{\partial k}{\partial z}\right) + G - \rho\varepsilon \quad (14)$$

And the equation for turbulence dissipation rate is given by:

$$\frac{\partial}{\partial x}(\rho u\varepsilon) + \frac{\partial}{\partial y}(\rho v\varepsilon) + \frac{\partial}{\partial z}(\rho w\varepsilon) = \frac{\partial}{\partial x}\left(\frac{\mu_t}{\sigma_\varepsilon}\frac{\partial k}{\partial x}\right) + \frac{\partial}{\partial y}\left(\frac{\mu_t}{\sigma_\varepsilon}\frac{\partial k}{\partial y}\right) + \frac{\partial}{\partial z}\left(\frac{\mu_t}{\sigma_\varepsilon}\frac{\partial k}{\partial z}\right) + (C_1 G - C_2\rho\varepsilon)\frac{\varepsilon}{k} \quad (15)$$

$$G = \mu_t\left[2\left(\left(\frac{\partial u}{\partial x}\right)^2 + \left(\frac{\partial v}{\partial y}\right)^2 + \left(\frac{\partial w}{\partial z}\right)^2\right) + \left(\frac{\partial u}{\partial y} + \frac{\partial v}{\partial x}\right)^2 + \left(\frac{\partial u}{\partial z} + \frac{\partial w}{\partial x}\right)^2 + \left(\frac{\partial v}{\partial z} + \frac{\partial w}{\partial y}\right)^2\right] \quad (16)$$

$$\mu_t = \frac{C_\mu \rho k^2}{\varepsilon} \quad (17)$$

The empirical constants (C_1, C_2, C_D, σ_k, σ_ε, C_μ) have been incorporated into the model, and their respective values are presented in Table 2. These constants have been effectively employed in numerous three-dimensional shapes.

Table 2. Constants values for the (*k-ε*) model [19].

C_1	C_2	C_D	σ_k	σ_ε	$C\mu$
1.44	1.92	1.0	1.0	1.3	0.09

4. Initial and boundary conditions

The typical boundary types encountered in the analysis of earth-coupled buildings include the soil surface and deep soil. Fig. 2 provides a detailed illustration of the initial and boundary conditions for the EAHE.

- **Initial conditions:**

1. For the temperature: the ambient temperature T_a = 313 K.
2. For the velocity: inlet velocity $V = V_{in}$ = (0.5, 1, 1.5, 2 m/s).

- **Boundary Conditions:**

1. The outlet boundary condition: pressure outlet boundary at atmospheric pressure (P = 0).
2. Boundaries surfaces of the pipe: $\partial T/\partial n \neq 0$, where: $n = x, y,$ and z direction.
3. All contact surfaces between soil and air are continuous boundary conditions as:

$$T_{air} = T_{soil} \rightarrow \left(-k\frac{\partial T}{\partial n}\right)_{air} = \left(-k\frac{\partial T}{\partial n}\right)_{soil}$$

Below are descriptions of the heat transfer processes occurring at these boundaries along with their mathematical models:

1. Deep soil conditions

Temperature conditions can be specified according to the circumstances and geographic location, as well as the data and time of 1/6/2023 at 12 p.m., according to equation (12) [5]:

$T = T(z, t)$ = 24.487 °C.

Where: z is the vertical coordinate at depth (3 m) and is assumed to be positive in the soil if conditions exist that maintain a constant temperature at a specific depth, then the specific temperature condition is considered appropriate for this case. As a result, many previous models assumed a constant temperature equal to the average dry bulb at great depth.

2. Soil surface

The boundaries of the soil surface are determined mathematically, as is the specified temperature condition.

$T = T_s$

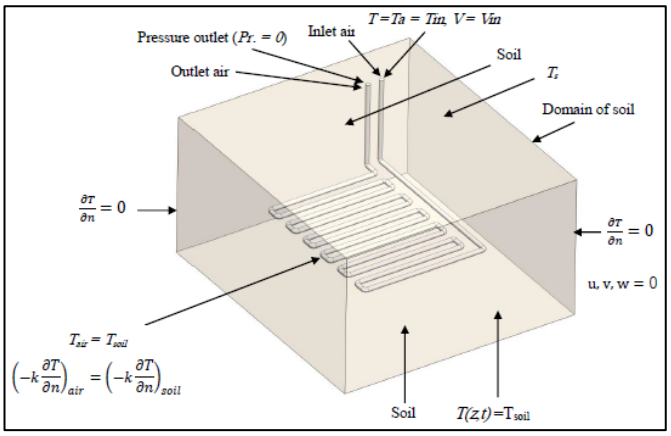

Fig. 2 Boundary types of domains for EAHE.

5. The Mesh

5.1. Mesh generation

The initial step in the finite volume method involves grid creation, where the working area is partitioned into smaller control volumes. Grid generation, a crucial aspect, finds numerous applications in computational fluid dynamics (CFD). The meshing process directly influences the accuracy and convergence of CFD simulation results [20]. For this study, the ANSYS-Fluent simulation program was utilized to fragment the generated model into smaller components using basic geometric elements, connected at shared nodes. Hexahedra were chosen for the pipe, while tetrahedra were selected for the soil. Higher mesh quality ensures more precise outcomes, though mesh quality below a certain threshold may yield inadequate results. Fig. 3 depicts the EAHE and displays various types of 3D mesh elements used in ANSYS-Fluent 2021/ R2.

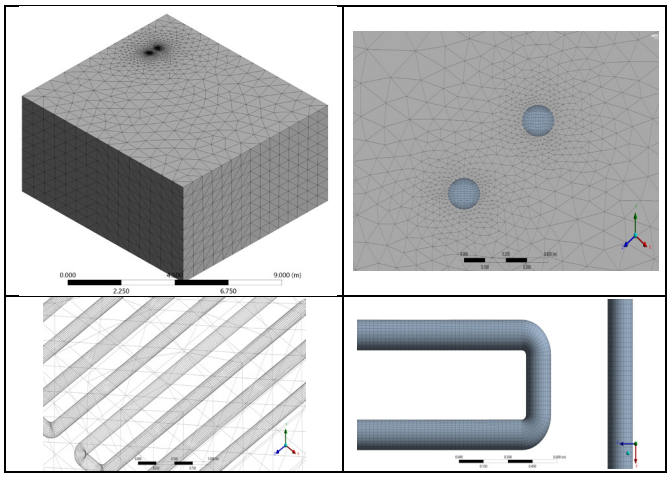

Fig. 3 Mesh generation for the whole domain of the EAHE, illustrating inlet and outlet openings.

5.2. Mesh independence test

To ensure that the outcomes are primarily influenced by the boundary conditions and physics applied rather than the mesh resolution, conducting a mesh independence analysis in computational fluid dynamics (CFD) is crucial. A widely adopted method to assess grid independence involves incrementally increasing resolution and conducting multiple simulations. If the results remain largely unchanged, it suggests that the initial grid is adequate. Calculations were executed for five distinct grid sizes, and the results of the grid independence test for heat exchange are summarized in Table 3.

It was observed that the findings and the obtained number of elements, 5,595,904 and 6,943,510, were nearly identical. Consequently, a domain comprising 5,595,904 elements was chosen to enhance computational accuracy and minimize calculation time. Fig. 4 explains the outlet temperature of the pipe with the number of elements.

Table 3. Grid independence test result for EAHE.

Mesh	No. of element	Outlet temperature (K)
Mesh – 1	1584221	310.7
Mesh – 2	3057655	309.9
Mesh – 3	4269665	308.8
Mesh – 4	5595904	308.266
Mesh – 5	6943510	308.24

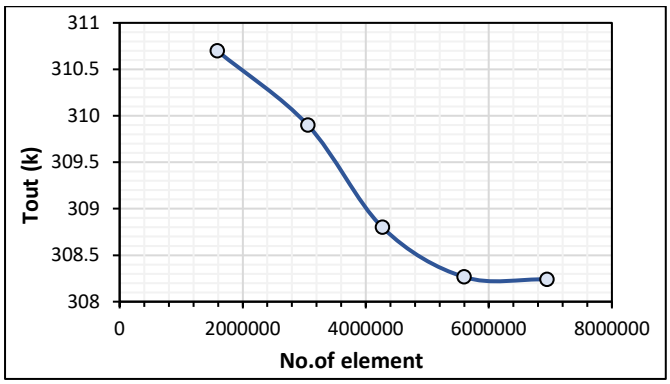

Fig. 4 Variation of pipe outlet temperature with total element number.

6. Numerical results validation

Before performing the theoretical analysis of the model using the ANSYS-Fluent 2021/R2 program, the correct operation of the program must be verified using experimental and theoretical data reported by Bansal et al. [21] and Bellatrache et al. [3] at different ambient temperatures. Table 4 shows the input parameters used for the researchers' model for the validation step, and the results are presented in Table 5 and Fig. 5. It can be noted that the results showed very good agreement between the theoretical and experimental results of previous studies, as the average outlet temperature was 3.89%, and this value falls within the error range and is considered a relatively low value. Therefore, we conclude that our model can correctly predict the thermal performance of the earth – air heat exchanger.

Table 4. Parameters entered for validation against theoretical and experimental results.

Parameter	Reference value
Pipe length	23.42 m
Pipe diameter	0.15 m
Soil density	2050 kg/m^3
Soil specific heat capacity	1840 J/kg. K
Soil thermal conductivity	0.52 W/m. °C
Soil temperature	26.7 °C

Table 5. Summary of outlet air temperature for present work comparing with theoretical and experimental data for previous studies.

Inlet air velocity (m/s)	Inlet air temperature (°C)	Outlet air temperature °C			Relative error % with Exp. data from [22]
		Exp. data from [22]	Theo. data from [3]	Theo. present work	
2	43.4	33.1	33.4	33.2	0.3
3	42.5	33.1	35.3	34.3	3.62
4	42.3	33.5	36.6	35.5	5.97
5	42.2	34.2	37.4	36.1	5.55

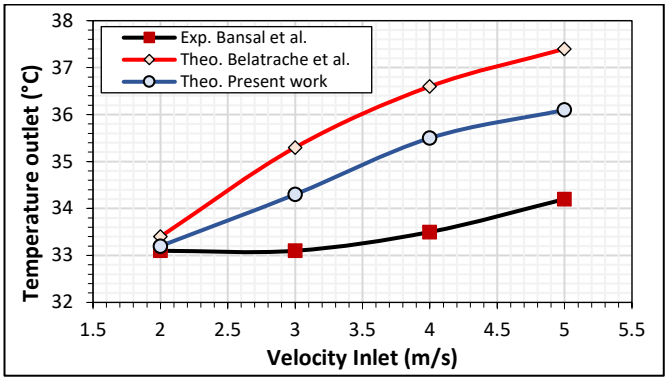

Fig. 5 Variation of velocity inlet with temperature outlet, pipe length = 23.42 m, pipe diameter = 0.15 m and T_{soil} = 26.7 °C, comparing with simulations and experiments for previous studies.

7. Results and discussion

The simulation analysis in this study was performed in Basrah city climate (longitude 47.749 and latitude 30.568) in Iraq by using ANSYS-Fluent 2021/R2 software. The results of EAHE and the performance of the pipe buried in the soil, including the different pipe diameters D = 7.62 cm (thickness = 2 mm), 10.16 cm (thickness = 2 mm), and 15.24 cm (thickness = 3 mm), different depths of pipe in the soil (Z = 1 m, 2 m, 3 m), and different velocities (v = 0.5 m/s, 1 m/s, and 1.5 m/s), are presented. All the models of cases subjected to the inlet temperature (ambient temperature) ($T_a = T_{in}$) to the EAHE are 313 K, the temperature of the surface (T_s) is 304.578 K, the temperature of the soil (T_{soil}) is 297.487 K at depth Z = 3 m, and the atmospheric pressure.

Figure 6 shows the contour of temperature distribution of the soil and pipe at pipe diameter (D = 7.62, 10.16, and 15.24 cm) and buried depth of pipe Z = 3 m for three inlet velocities (v = 0.5, 1, and 1.5 m/s).

At D = 7.62 cm, it can be seen that the temperature increases with increasing velocity due to an increase in heat transfer rate with increasing mass flow rate, where the temperature of the inlet air is greater than the temperature of the soil.

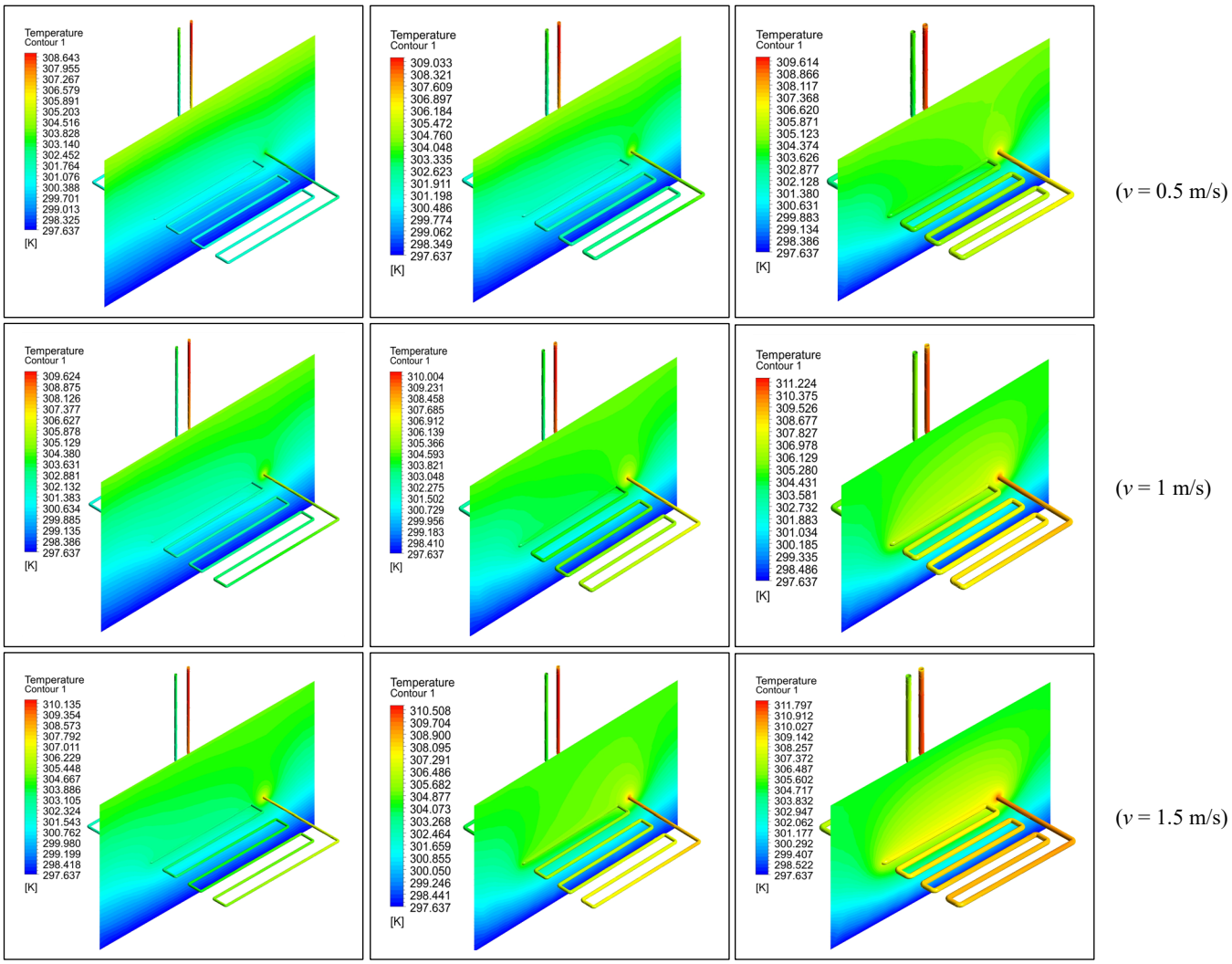

Fig. 6 Contours illustrate the temperature distribution for the soil and inside the pipe at buried depth (Z) = 3 m, different pipe diameter and with different velocity.

The effect of pipe diameters D = 10.16 cm and D = 15.24 cm indicates that with increasing diameter, the temperature increases, which returns to increase the mass flow rate (inlet mass of air) with diameter, which causes an increase in heat transfer to the pipe and soil. When the velocity v = 1 m/s, the maximum temperature at D = 7.62 cm is 309.624 K, at D = 10.16 cm is 310.004 K, and at D = 15.24 cm is 311.224 K. We notice from this figure, at D = 7.62 cm, that the maximum temperature is lower than the maximum temperature when D = 10.16 cm and D = 15.24 cm. Also, from the vertical section, the temperature of the soil is graduated from the minimum value at the bottom (297.637 K) to the maximum value at the surface of the soil and inlet pipe. We note from the figure that the smaller the diameter, the lower the outlet temperature from the pipe, and this leads to improved ventilation.

Fig. 7 shows the contour of velocity distribution for the pipe at pipe diameter (D = 7.62, 10.16, and 15.24 cm) and buried depth of pipe Z = 3 m for three inlet velocities (v = 0.5, 1, and 1.5 m/s). It can be seen that the maximum velocity increases with increasing inlet velocity; for example, at D = 7.62 cm, the maximum velocity is 0.791 m/s, 1.562 m/s, and 2.337 m/s for inlet velocity 0.5 m/s, 1 m/s, and 1.5 m/s, respectively. From this figure, it can be concluded that the effect of depth on velocity is small, where the properties of fluids are constant (not varying with temperature). We note from the velocity distribution contours inside the pipe that the effect of depth on velocity has a small effect when the properties of the air are constant (do not change with temperature). As for changing diameters, as the diameter increases, the velocity increases by a small percentage; for example, at v = 1.5 m/s, the maximum velocity is 2.337 m/s, 2.346 m/s, and 2.543 m/s for D = 7.62 cm, 10.16 cm, and 15.24 cm, respectively.

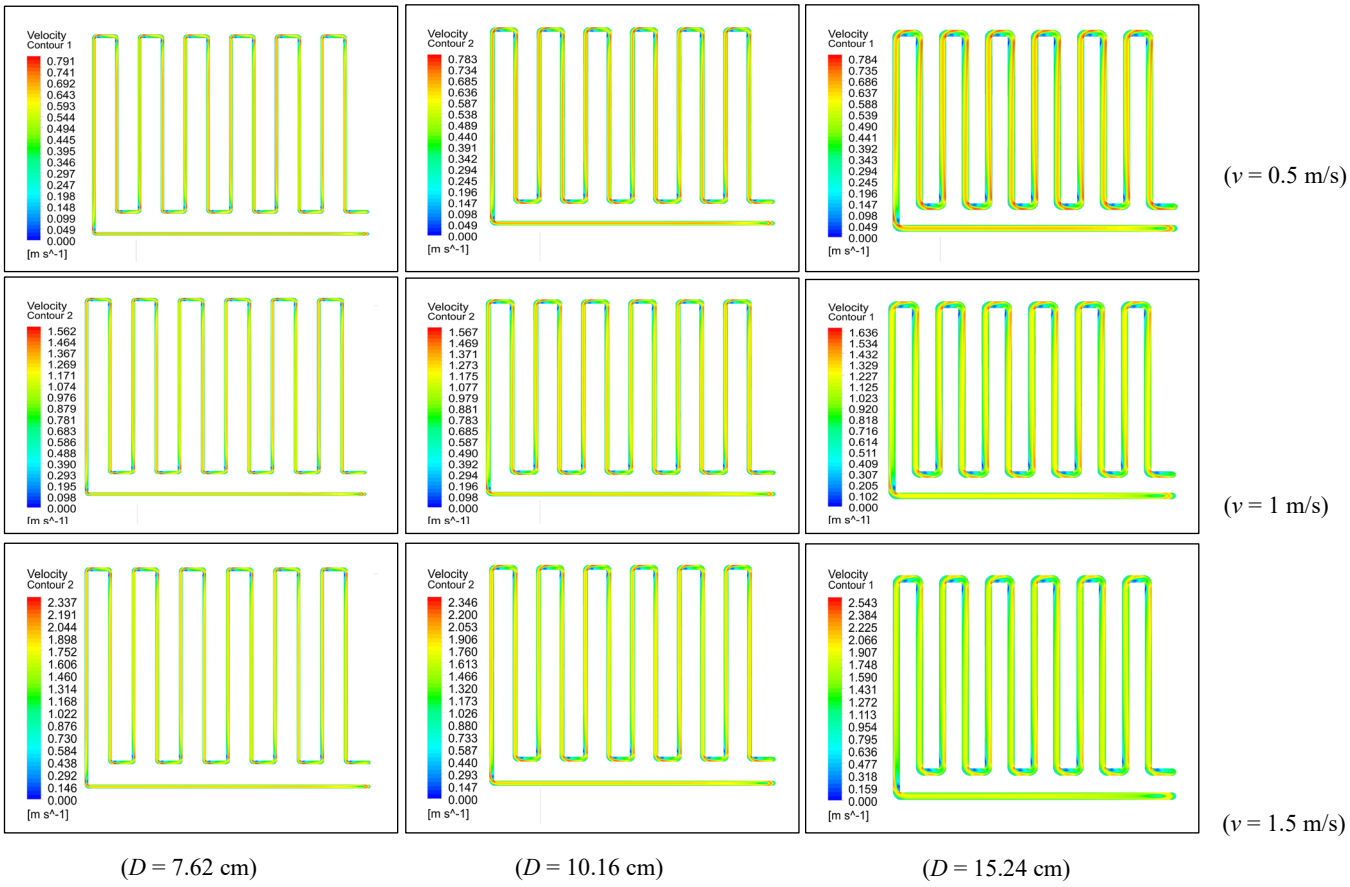

Fig. 7 Contours illustrate the velocity distribution inside the pipe at buried depth (Z) = 3 m, different pipe diameter and with different velocity.

Figure 8 illustrates the temperature distribution of soil with depth (Z) in the soil at diameter D = 7.62 cm and buried pipe depth Z = 1 m, 2 m, and 3 m for three velocities (v = 0.5, 1, and 1.5 m/s). It can be seen that increasing velocity increases the temperature of the soil because it increases the heat transfer rate (conduction) where the temperature of the air is greater than the temperature of the soil. Also, the general trend of soil temperature with depth is decreasing with all velocities, indicating that return to the temperature of the soil surface, which is always greater than the soil temperature and decreases with depth. At depth Z = 1, where the pipe is buried, the temperature increases and then decreases due to the flow of air. The effect of anther depths Z = 2 m and Z = 3 m. These figures indicate that, with increasing depth, the temperature of the soil at the depth of the buried pipe decreases with increasing depth. The maximum outlet temperature of the pipe at the buried depth (Z = 1, 2, and 3) m at velocity 1.5 m/s, and D = 7.62 cm are: 304.487 K, 304.042 K, and 303.216 respectively. And the thermal exchange between the air crossing the pipe and soil increases with the length of buried pipe.

Figure 9 shows the temperature distribution of soil for three depths of buried pipe Z = 1 m, 2 m, and 3 m, respectively, at diameter D = 10.16 cm, for three velocities (v = 0.5, 1, 1.5, and 2 m/s). These figures show that increasing the diameter results in an increase in the temperature of the soil and the outlet temperature of the air, which in turn decreases the heat transfer (conduction) with the diameter of the pipe.

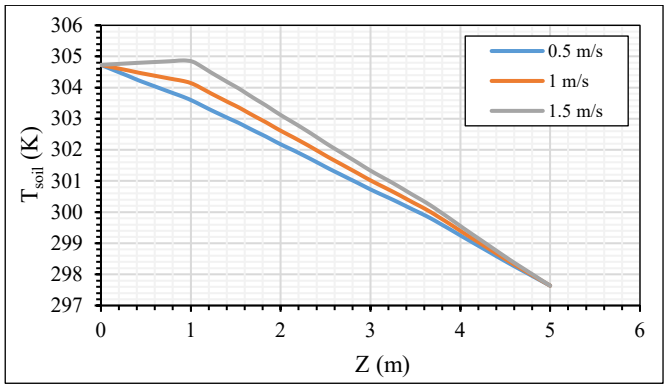

(a) Z = 1 m.

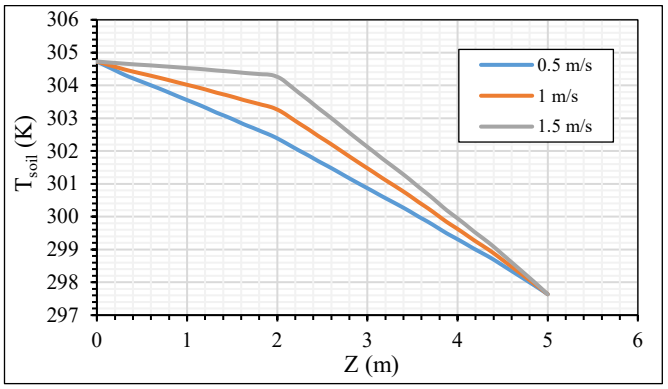

(b) Z = 2 m.

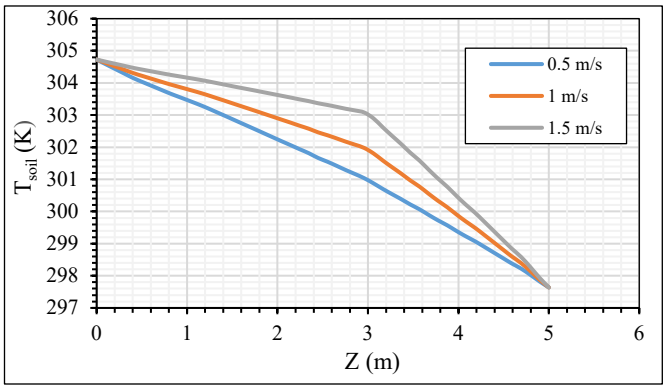

(c) Z = 3 m.

Fig. 8 Temperature distribution for the soil at pipe diameter D = 7.62 cm and different buried pipe Z = 1 m, 2 m, and 3 m with different velocity v = 0.5 m/s, 1 m/s, and 1.5 m/s.

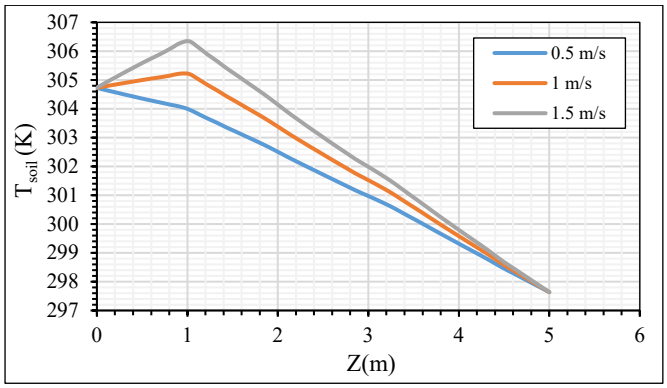

(a) Z = 1 m.

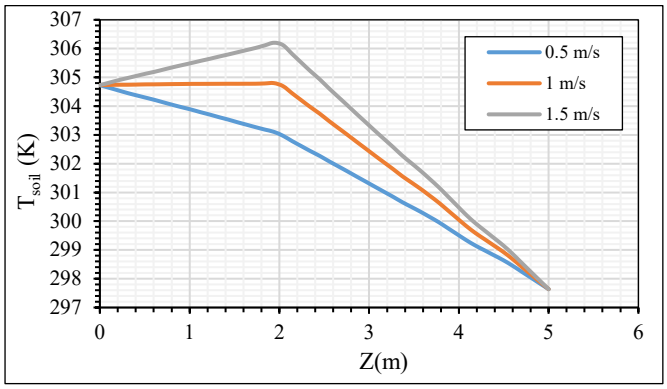

(b) Z = 2 m.

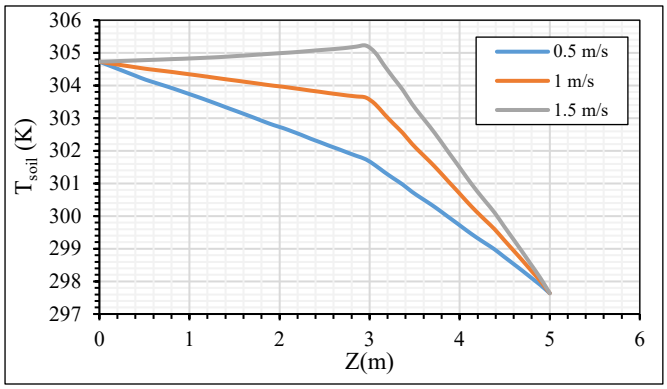

(c) Z = 3 m.

Fig. 9 Temperature distribution for the soil at pipe diameter D = 10.16 cm and different buried pipe Z = 1 m, 2 m, and 3 m with different velocity v = 0.5 m/s, 1 m/s, and 1.5 m/s.

Figure 10 shows the temperature distribution of the soil for three depths of buried pipe Z = 1 m, 2 m, and 3 m, respectively, at diameter D = 15.24 cm, for three velocities (v = 0.5, 1, 1.5, and 2 m/s). It can be seen from these figures that increasing the diameter results in an increase in the temperature of the soil and the outlet temperature of the air, which in turn decreases the heat transfer (conduction) with the diameter of the pipe. When the diameter increases, the outlet temperature of the pipe increases because the heat transfer coefficient by convection decreases. Therefore, as the diameter of the pipe decreases, the temperature decreases.

Figure 11 depicts the variation in air temperature distribution along the pipe at three different buried depths of Z = 1 m, 2 m, and 3 m, respectively, with a diameter of D = 7.62 cm and for three velocities (v = 0.5, 1, and 1.5) m/s. This figure illustrates that air velocity influences the outlet air temperature of the heat exchanger, with lower velocities resulting in a decreased outlet air temperature.

Additionally, the temperature within the pipe gradually decreases until it approaches the soil temperature. At a depth of 3 m and a velocity of 1 m/s, the temperature decreases from the ambient temperature (313 K) until it nears the soil temperature, approximately 301.2 K. Moreover, it's evident that as the depth increases, the outlet temperature of the heat exchanger decreases. Beyond a length of 29 m, the air temperature inside the heat exchanger remains constant.

Figure 12 shows the variation of the air temperature distribution along the pipe for three buried depths of pipe Z = 1 m, 2 m, and 3 m, respectively, at diameter D = 10.16 cm for three different velocities (v = 0.5, 1, and 1.5) m/s. It can be seen from this figure that the air velocity affects the air temperature of the pipe outlet, as increasing the velocity increases the outlet air temperature of the heat exchanger. We also notice that the temperature inside the pipe begins to decrease until it becomes close to the temperature of the soil.

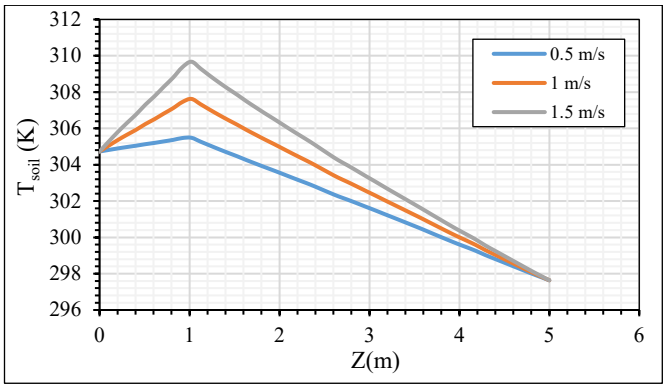

(a) Z = 1 m.

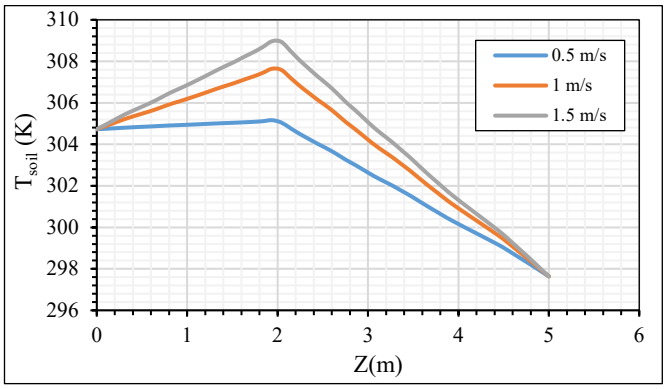

(b) Z = 2 m.

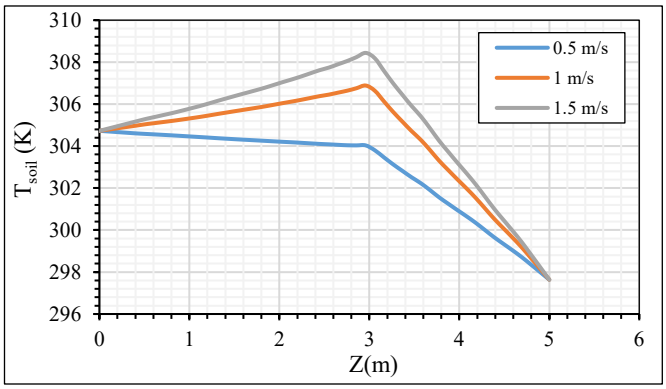

(c) Z = 3 m.

Fig. 10 Temperature distribution for the soil at pipe diameter D = 15.24 cm and different buried pipe Z = 1 m, 2 m, and 3 m with different velocity v = 0.5 m/s, 1 m/s, and 1.5 m/s.

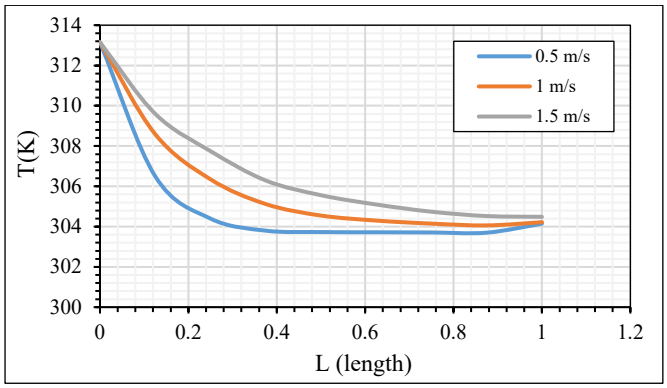

(a) Z = 1 m.

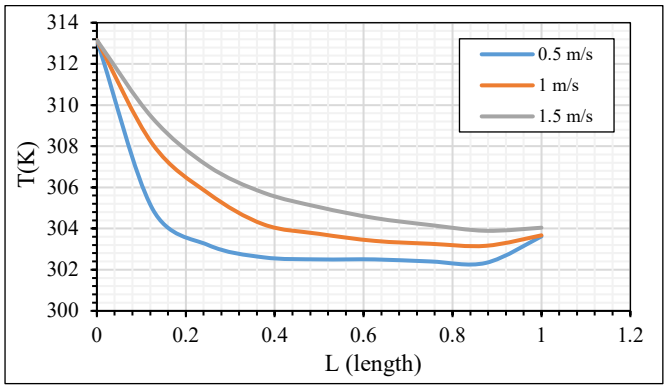

(b) Z = 2 m.

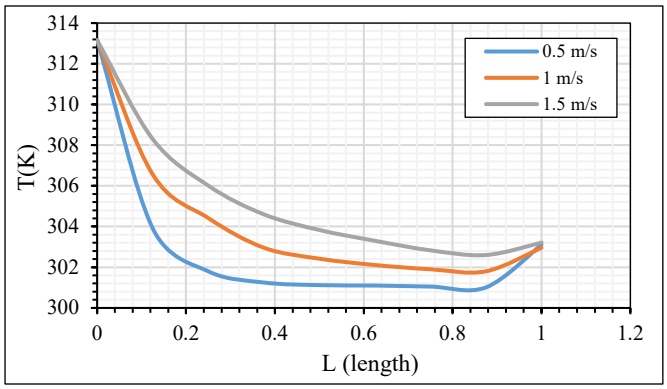

(c) Z = 3 m.

Fig. 11 Temperature distribution along the pipe at pipe diameter D = 7.62 cm and different buried pipe Z = 1 m, 2 m, and 3 m with different velocity v = 0.5 m/s, 1 m/s, and 1.5 m/s.

At depth 3 m and velocity 0.5 m/s, we notice that the temperature decreases from the ambient temperature, which is 313 K, until it reaches approximately the soil temperature, about 303.014 K. We can also notice that as the depth increases, the outlet temperature of the heat exchanger decreases. Moreover, the air temperature inside the heat exchanger decreases by a small percentage beyond a length of 36 m.

Figure 13 illustrates the variation in air temperature distribution along the pipe at three different buried depths of Z = 1 m, 2 m, and 3 m, respectively, with a diameter of D = 15.24 cm and three various velocities (v = 0.5, 1, and 1.5) m/s. It can be seen from this figure that air velocity impacts the outlet air temperature of the heat exchanger, with higher velocities resulting in an increased outlet air temperature. Moreover, it's observed that the temperature within the pipe gradually decreases until it approaches the soil temperature.

At a depth of 3 m and a velocity of 0.5 m/s, the temperature decreases from the ambient temperature (313 K) until it approaches the soil temperature, approximately 303.752 K. Additionally, it's noted that as the depth increases, the outlet temperature of the heat exchanger decreases. The air temperature inside the heat exchanger experiences a slight decrease beyond a length of 50 m because the diameter is bigger than that at D = 7.62 cm and D = 10.16 cm, which means more flow rate enters the pipe, which leads to a decrease in heat transfer between the air inside the pipe and the soil outside the pipe.

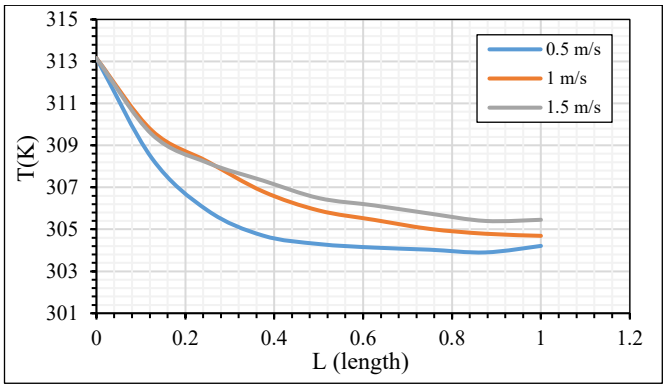

(a) Z = 1 m.

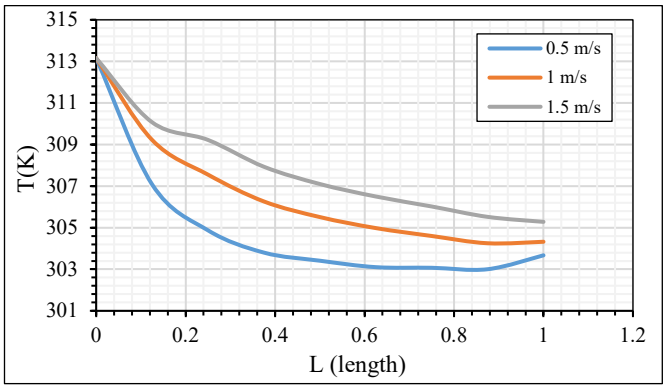

(b) Z = 2 m.

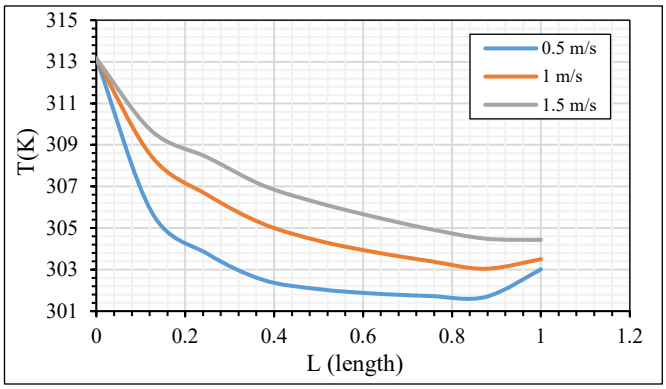

(c) Z = 3 m.

Fig. 12 Temperature distribution along the pipe at pipe diameter D = 10.16 cm and different buried pipe Z = 1 m, 2 m, and 3 m with different velocity v = 0.5 m/s, 1 m/s, and 1.5 m/s.

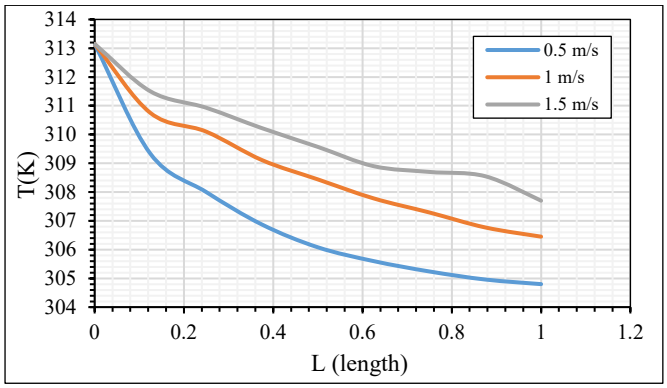

(a) Z = 1 m.

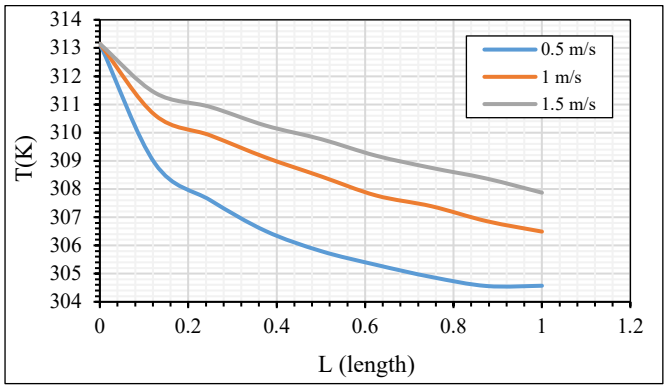

(b) Z = 2 m.

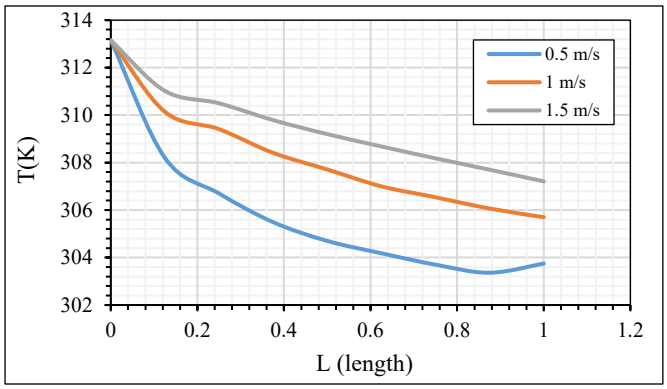

(c) Z = 3 m.

Fig. 13 Temperature distribution along the pipe at pipe diameter D = 15.24 cm and different buried pipe Z = 1 m, 2 m, and 3 m with different velocity v = 0.5 m/s, 1 m/s, and 1.5 m/s.

The effect of pipe diameter D = 7.62, 10.16, and 15.24 cm on the temperature distribution for the soil with buried pipe Z = 3 m and inlet velocity v = 1 m/s is shown in Fig. 14. It can be seen from this figure that when the diameter of the pipe decreases, the temperature of the soil decreases, and this leads to an increase in the air outlet temperature from the heat exchanger. The reason for this is that the larger diameter of the pipe reduces the heat transfer coefficient by convection, and this leads to an increase in the temperature of the air outlet of the heat exchanger. Therefore, a smaller pipe diameter has better performance. When the diameter is small, the center of the pipe is close to the soil outside, and this allows more heat to be transferred from the air inside the pipe to the soil.

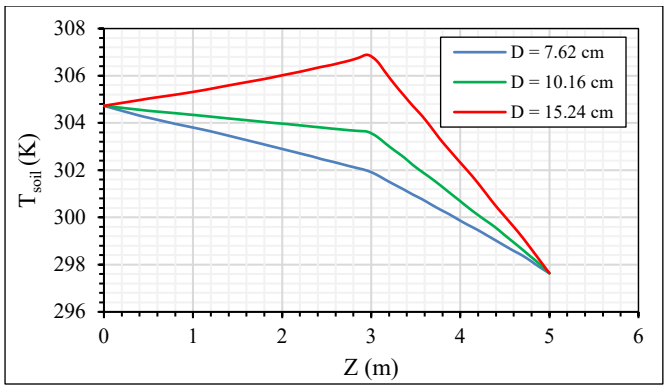

Fig. 14 Temperature distribution for the soil with buried pipe Z = 3 m at v = 1 m/s and different pipe diameter.

The effect of pipe diameter D = 7.62, 10.16, and 15.24 cm on the temperature distribution along the pipe with buried pipe Z = 3 m and inlet velocity v = 1 m/s is shown in Fig. 15. It can be observed from this figure that with a decrease the pipe diameter, the temperature inside the pipe decreases. As the diameter of the pipe decreases, the heat transfer coefficient by convection increases because the center point of the pipe is closer to the soil outside.

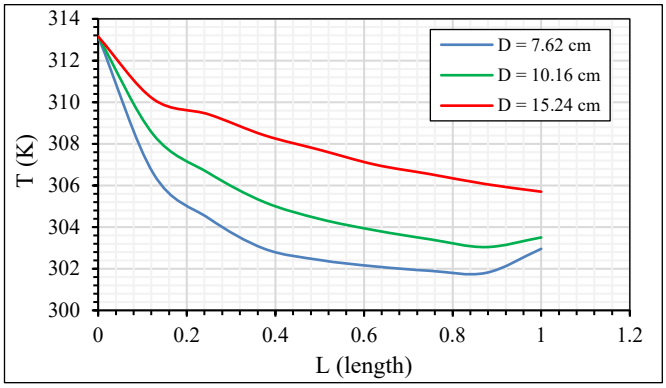

Fig. 15 Temperature distribution along the pipe with buried pipe Z = 3 m at v = 1 m/s and different pipe diameter.

Figure 16 displays the influence of pipe diameter D = 7.62, 10.16, and 15.24 cm on the outlet temperature of the pipe with velocity at a buried depth of Z = 3 m. It's evident from this figure that air velocity impacts the outlet air temperature of the heat exchanger, with higher velocities resulting in an increased outlet air temperature. Additionally, it's observed that as the diameter increases, the outlet air temperature of the heat exchanger rises due to the increased mass flow rate. Consequently, this leads to a decrease in the heat transfer coefficient by free convection due to the increased distance between the center of the pipe and the surrounding soil.

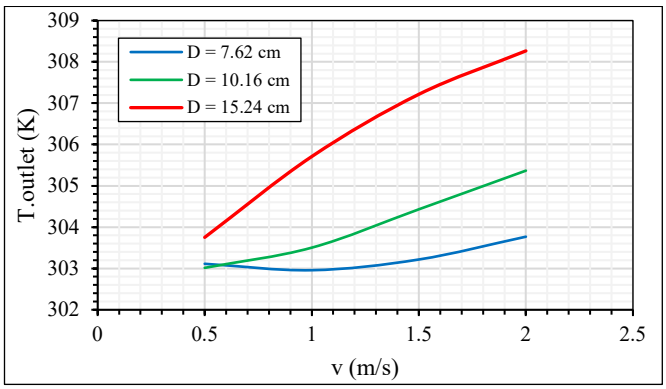

Fig. 16 Temperature outlet for the pipe with velocity at: buried pipe Z = 3 m and different diameter.

8. Conclusion

The current investigation focuses on exploring the impact of soil temperature on the Earth-Air Heat Exchanger in Basrah city, Iraq, employing both numerical and theoretical analyses. Numerical simulations were conducted using ANSYS-Fluent 2021/R2 to examine various factors such as the diameter of the buried pipe, the depth of burial of the heat exchanger, and the velocity of air entering the heat exchanger on the outlet air temperature from the pipe, soil temperature, velocity distribution, and temperature distribution. The basic findings of the current study can be summarized as follows:

1. As the depth of the buried pipe decreases, the temperature of the air outlet the heat exchanger increases. This occurs because the soil temperature increases nearer to the soil surface, leading to a temperature decline as we move away from it.
2. As the diameter decreases, the air outlet temperature from the heat exchanger and the soil temperature decreases due to increased heat transfer. This is due to the fact that when the pipe diameter is small, the center point of the pipe is close to the soil surface.
3. Air flow or air inlet velocity must be appropriate, as the best velocity is 1 m/s, and as the velocity increases, the difference between the inlet and outlet temperatures of the heat exchanger is smaller.
4. Changing diameters has very little effect on the velocity of air inlet.
5. The effect of depth on velocity is very small when the fluid properties are constant, i.e., there is no change with temperature.
6. When the velocity increases, the soil temperature increases due to the increase in the rate of heat transfer, as the temperature of the air inlet the heat exchanger is higher than the temperature of the soil.
7. The temperature inside the heat exchanger begins to decrease until it becomes close to the temperature of the soil, especially at a depth of 3 m, when the length of the pipe is about 30 m. After this length, the decrease in temperature is very small.
8. The maximum temperature difference of about 10 °C between the ambient temperature and the outlet temperature of the heat exchanger was obtained at a depth of 3 m and a velocity of 1 m/s at a diameter of 7.62 cm.

References

[1] S. N. Ahmed and O. Prakash, “Thermal performance evaluation of an earth-to-air heat exchanger for the heating mode applications using an experimental test rig”, archives of thermodynamics, Vol. 43, No. 1, pp. 185-207, 2022. https://doi.org/10.24425/ather.2022.140931

[2] I. D. Anikina, V. V. Sergeyev, N. T. Amosov, and M. G. Luchko, “Use of heat pumps in turbogenerator hydrogen cooling systems at thermal power plant”, International Journal of Hydrogen Energy, Vol. 42, Issue 1, pp. 636-642, 2017. https://doi.org/10.1016/j.ijhydene.2016.04.256

[3] D. Belatrache, S. Bentouba, and M. Bourouis, “Numerical analysis of earth air heat exchangers at operating conditions in arid climates”, International Journal of Hydrogen Energy, Vol. 42, Issue 13, pp. 8898-8904, 2017. http://doi.org/10.1016/j.ijhydene.2016.08.221

[4] A. H. Poshtiri, N. Gilani, and F. Zamiri, “Feasibility study on using solar chimney and earth-to-air heat exchanger for natural heating of buildings”, World Renewable Energy Congress, 2011.

[5] S. H. Hammadi and A. H. Mohammed, “Application of Earth Tube Heat Exchanger and Solar Chimney for Natural Cooling System in Basrah City”, Basrah Journal for Engineering Sciences, Vol. 14, 2014.

[6] H. Li, Y. Yu, F. Niu, M. E. Shafik, and B. Chen, "Performance of a Coupled Cooling System with Earth-to-Air Heat Exchanger and Solar Chimney", Renewable Energy, Vol. 62, pp. 468-477, 2014. http://doi.org/10.1016/j.renene.2013.08.008

[7] A. P. Haghighi and M. Maerefat, "Design guideline for application of earth-to-air heat exchanger coupled with solar chimney as a natural heating system", International Journal of Low-Carbon Technologies, Vol. 10, Issue 3, pp. 294-304, 2015. http://doi.org/10.1093/ijlct/ctu006

[8] A. A. Serageldina, A. Abdeenb, M. M. S. Ahmed, A. Radwand, A. N. Shmroukhe, S, Ookawara, "Solar chimney combined with earth-to-air heat exchanger for passive cooling of residential buildings in hot areas", Solar Energy, Vol. 206, pp. 145-162, 2020. https://doi.org/10.1016/j.solener.2020.05.102

[9] S. F. Ahmed, G. Liu, M. Mofijur, A. K. Azad, M. A. Hazrat, Y.-M. Chu, "Physical and hybrid modelling techniques for earth-air heat exchangers in reducing building energy consumption: Performance, applications, progress, and challenges", Solar Energy, Vol. 216, pp. 274-294, 2021. https://doi.org/10.1016/j.solener.2021.01.022

[10] A. Mostafaeipour, H. Goudarzi, M. Khanmohammadi, M. Jahangiri, A. Sedaghat, H. Norouzianpour, S. Chowdhury, K. Techato, A. Issakhov, K. Almutairi, and S. J. H. Dehshiri, "Techno-economic analysis and energy performance of a geothermal earth-to-air heat exchanger (EAHE) system in residential buildings: A case study", Energy Science & Engineering, Vol. 9, Issue 10, pp. 1807-1825, 2021. https://doi.org/10.1002/ese3.952

[11] T. M. Essa and S. H. Hammadi, "Effect of solar radiation and soil temperature on the flow characteristics in above ground and underground petroleum pipelines", Basrah Journal for Engineering Sciences, Vol. 23, No. 2, pp. 50-57, 2023. https://doi.org/10.33971/bjes.23.2.7

[12] F. M. Abed, M. H. Zaidan, Y. H. Hussein and A. K. Jassim, "Passive air-conditioning of domestic using a hybrid system of solar updraft tower and a geothermal in Tikrit city-Iraq", IOP Conference Series: Materials Science and Engineering, 1058, 2021. https://doi.org/10.1088/1757-899X/1058/1/012057

[13] A. A. Serageldina, A. K. Abdelrahman, S. Ookawara, "Parametric study and optimization of a solar chimney passive ventilation system coupled with an earth-to-air heat exchanger", Sustainable Energy Technologies and Assessments, Vol. 30, pp. 263-278, 2018. https://doi.org/10.1016/j.seta.2018.10.010

[14] B. Buonomo, L. Capasso, A. Diana, O. Manca and S. Nardini, "A numerical analysis on a solar chimney with an integrated latent heat thermal energy storage", AIP Conference Proceedings, Vol. 2191, Issue 1, 2019. https://doi.org/10.1063/1.5138762

[15] H. K. Versteeg and W. Malalasekera, An introduction to computational fluid dynamics, British Library Cataloguing-in-Publication Data, ISBN: 978-0-13-127498-3, 2007. www.pearsoned.co.uk/versteeg

[16] A. Pasupath, L. Athanasius, R. Velraj, and R. V. Seeniraj, "Experimental investigation and numerical simulation analysis on the thermal performance of a building roof incorporating phase change material (PCM) for thermal management", Applied Thermal Engineering, Vol. 28, Issue 5-6, pp. 556-565, 2008. https://doi.org/10.1016/j.applthermaleng.2007.04.016

[17] T. Kusuda and P. R. Achenbach, "Earth Temperature and Thermal Diffusivity at Selected Stations in United States", National Bureau of Standards Report, Ashrae Transactions, Part 1, 1965.

[18] T. S. Bisoniya, "Design of earth–air heat exchanger system", Geothermal Energy, Vol. 3, Issue 18, 2015. https://doi.org/10.1186/s40517-015-0036-2

[19] B. E. Launder and D. B. Spalding, "The numerical computation of turbulent flows", Computer Methods in Applied Mechanics and Engineering, Vol. 3, Issue 2, pp. 269-289, 1974. https://doi.org/10.1016/0045-7825(74)90029-2

[20] J. F. Thompson, B. K. Soni, and N. P. Weatherill, Hand book of grid generation, ISBN 0-8493-2687-7, 1999.

[21] V. Bansal, R. Mishra, G. D. Agarwal, and J. Mathur, "Performance analysis of integrated earth-air-tunnel-evaporative cooling system in hot and dry climate", Energy and Buildings, Vol. 47, pp. 525-532, 2012. https://doi.org/10.1016/j.enbuild.2011.12.024